



DEPARTMENT OF MATHEMATICAL SCIENCES

TMA4212 - NUMERICAL SOLUTION OF DIFFERENTIAL EQUATIONS BY
DIFFERENCE METHODS

Heat Distribution in Anisotropic Materials

Authors:

Peder Brekke
Simen Nesland
Espen Bjørge Urheim

02.26.2023

Introduction

In this project, we aim to investigate heat distribution in anisotropic materials and solve the associated Poisson equation numerically. First, we will focus on two-dimensional models with two distinguished directions for heat flow with differing conductivity. We will discretize and solve the problem numerically using central differences and experiment with different boundary conditions and heat sources. We will then perform some theoretical analysis to find an error bound for the scheme, and compare with our numerical results. We will then solve the Dirichlet boundary value problem for the Poisson equation in a specified domain. Here we will investigate two strategies for handling irregular boundaries and compare their effectiveness and efficiency.

1 Anisotropic Heat Distribution on a Rectangular Domain

We start by looking at anisotropic materials where heat flows faster in the directions $\vec{d}_1 = (1, 0)$ and $\vec{d}_2 = (1, r)$. The Poisson equation we want to solve therefore becomes

$$-\nabla \cdot (\kappa \nabla T) = -(a + 1)\partial_x^2 u - 2r\partial_x\partial_y u - r^2\partial_y^2 u = -a\partial_x^2 u - (\nabla \cdot \vec{d}_2)u = f,$$

which we will discretize, analyse and test numerically on the rectangular domain $\Omega = [0, 1] \times [0, 2]$.

1.1 Discretization with $r = 2$

We divide the rectangular domain Ω into M sub-intervals in x -direction, and define our step length $h = \frac{1}{M}$. In y -direction, we let $k = |r|h$ be our step length, where $r \in \mathbb{R}$; initially set to $r = 2$. Now we have created our grid $\overline{\mathbb{G}}$, which consists of inner points \mathbb{G} and a boundary $\partial\mathbb{G}$.

Discretized mixed derivatives are numerically unstable, and therefore we want to discretize the second order directional derivatives instead,

$$-\mathcal{L}u_P = -a\partial_x^2 u_P - (\vec{d}_2 \cdot \nabla)^2 u_P = f_P. \quad (1)$$

For this we use second order central differences. Denoting $u(x, y) = u_P$, $u(x + h, y) = u_{E'}$, $u(x - h, y) = u_{W'}$, $u(x + h, y + rh) = u_{NE'}$ and $u(x - h, y - rh) = u_{SW'}$, the scheme becomes

$$-\mathcal{L}_h u_P = \frac{a}{h^2}(-u_{W'} + 2u_P - u_{E'}) - \frac{1}{h^2}(\alpha u_{SW'} + \beta u_P + \gamma u_{NE'}). \quad (2)$$

The coefficients α , β and γ can be determined by Taylor-expansion of u_Q , $Q = SW', NE'$ around u_P , with the intention of having a local truncation error

$$\tau_P = \mathcal{L}_h u_P - \mathcal{L}u_P = O(h^2). \quad (3)$$

In the x -direction, the local truncation error of the second order central difference scheme is known to be

$$\tau_{\vec{d}_1} = \frac{ah^2}{12}\partial_x^4 u + O(h^4) = O(h^2).$$

In the \vec{d}_2 -direction, we have

$$\tau_{\vec{d}_2} = \frac{1}{h^2} (\alpha u_{SW'} + \beta u_P + \gamma u_{NE'}) - \partial_x^2 u - 2r\partial_x\partial_y u - r^2\partial_y^2 u \quad (4)$$

where

$$u_{NE'} = u + (h\partial_x + rh\partial_y)u + \frac{1}{2}(h\partial_x + rh\partial_y)^2 u + \frac{1}{6}(h\partial_x + rh\partial_y)^3 u + \frac{1}{24}(h\partial_x + rh\partial_y)^4 u + O(h^5)$$

$$u_{SW'} = u - (h\partial_x + rh\partial_y)u + \frac{1}{2}(h\partial_x + rh\partial_y)^2 u - \frac{1}{6}(h\partial_x + rh\partial_y)^3 u + \frac{1}{24}(h\partial_x + rh\partial_y)^4 u + O(h^5)$$

In order to achieve consistency of order 2, we see from (4) that we need the first, second and third derivatives to cancel out. Since the first and third derivatives only appear in the Taylor expansions, with opposite signs, we conclude that $\alpha = \gamma$. For the second derivatives, we get that

$$\frac{\alpha + \gamma}{2}(\partial_x^2 u + 2r\partial_x\partial_y u + r^2\partial_y^2 u) - \partial_x^2 u - 2r\partial_x\partial_y u - r^2\partial_y^2 u = 0 \Rightarrow \frac{\alpha + \gamma}{2} = 1 \Rightarrow \alpha = \gamma = 1$$

To get rid of the u -term we need $\alpha + \beta + \gamma = 0$, which means that $\beta = -2$. Inserting for α , β and γ in (2), we find that the final discretised equation is

$$-\mathcal{L}_h U_P = \frac{1}{h^2} ((2 + 2a)U_P - aU_{W'} - aU_{E'} - U_{SW'} - U_{NE'}). \quad (5)$$

1.2 Implementation

Using (5), we implement the scheme in matrix form, where we obtain the block tridiagonal matrix A_h ,

$$A_h = \begin{bmatrix} B & C & 0 \\ C^\top & B & \ddots \\ 0 & \ddots & \ddots \end{bmatrix} \text{ where } B = \begin{bmatrix} 2 + 2a & -a & 0 \\ -a & 2 + 2a & \ddots \\ 0 & \ddots & \ddots \end{bmatrix}, \quad C = \begin{bmatrix} 0 & -1 & 0 \\ 0 & 0 & \ddots \\ 0 & \ddots & \ddots \end{bmatrix},$$

and solve the equation $A_h U = h^2 f + g$ for U to find our numerical solution.

In this short section we focus on the numerical solution, and the effects of adjusting the parameter a . We set the boundaries to zero and use a bell-curve, $f(x, y) = 50e^{-10(x-0.5)^2}e^{-10(y-1)^2}$, as the heat source. Using $a = 0.5$ and $a = 10$ we run our solver. Figure 2 shows the results. From the plot using $a = 0.5$ we clearly see how the $(1, r) = (1, 2)$ direction dominates the heat flow, while the opposite effect is observed for $a = 10$. This is the expected result as $R \propto a$, where R is the relative conductivity of \vec{d}_1 versus \vec{d}_2 . Also, greater a gives greater average conductivity, so it makes sense that the plot with $a = 0.5$ has greater temperature. Our solver seems to be stable and the results are in compliance with theory. Additional plots with more experimental boundary conditions are added in the appendix.

1.3 Monotonicity

We now look at monotonicity as a first step towards finding an error bound for the scheme, which we later can test numerically. A numerical scheme is monotone if it satisfies the discrete maximum principle (DMP), which it does if it has positive coefficients and is boundary connected. Using equation (5), and looking at the general form of a numerical scheme,

$$-\mathcal{L}_h U_P = \alpha_{PP} U_P - \sum_Q \alpha_{PQ} U_Q,$$

we immediately see that all coefficients are positive, and that

$$\alpha_{PP} - \sum_Q \alpha_{PQ} = 2 + 2a - a - a - 1 - 1 \geq 0.$$

Hence we conclude that it has positive coefficients. Next, looking at the stencil of the scheme (shown in figure 1), we see that any point $Q \in \partial\mathbb{G}$ can be reached from any point $P \in \mathbb{G}$, so the scheme is boundary connected. Since the two criteria are fulfilled, the scheme satisfies DMP and is monotone.

1.4 L^∞ -stability

In order to prove convergence and find an error bound on our scheme, we also need to prove L^∞ -stability. To do so, we use the comparison function $\phi(x) = \frac{1}{2}x(1-x)$, and look at a solution V_P with zero at its boundary and a right hand side f , i.e.

$$-\mathcal{L}_h V_P = f, \quad V_P = 0 \text{ if } P \in \partial\mathbb{G}.$$

We define $W_P = V_P - \phi_P \|f\|_{L^\infty}$ such that

$$-\mathcal{L}_h W_P = -\mathcal{L}_h V_P - (-\mathcal{L}_h \phi_P) \|f\|_{L^\infty} = f - (-\mathcal{L}_h \phi_P) \|f\|_{L^\infty},$$

where (4) and Taylor-expansion around x gives

$$\begin{aligned} -\mathcal{L}_h \phi_P &= \frac{1}{h^2} ((2+2a)\phi(x) - a\phi(x-h) - a\phi(x+h) - \phi(x-h) - \phi(x+h)) \\ &= \frac{1}{h^2} ((2+2a)\phi(x) - 2a\phi(x) - ah^2\phi''(x) - 2\phi(x) - h^2\phi''(x)) = 1+a > 1. \end{aligned}$$

Hence, we end up with

$$-\mathcal{L}_h W_P = f - (-\mathcal{L}_h \phi_P) \|f\|_{L^\infty} = f - (1+a) \|f\|_{L^\infty} \leq 0,$$

which means that DMP is satisfied. Thus, we have

$$W_P = V_P - \phi_P \|f\|_{L^\infty} \leq \max_{P \in \partial\mathbb{G}} \{V_P - \|f\|_{L^\infty} \phi_P, 0\},$$

and since $\phi(x) \geq 0$ when $x \in [0, 1]$ and $V_P = 0$ if $P \in \partial\mathbb{G}$,

$$V_P - \phi_P \|f\|_{L^\infty} \leq 0 \Rightarrow V_P \leq \|f\|_{L^\infty} \max_{x \in [0,1]} \phi_P = \frac{1}{8} \|f\|_{L^\infty}$$

Next, if we perform the mapping $V, f \mapsto -V, -f$, the exact same analysis yields

$$\max_{P \in \mathbb{G}} (-V_P) \leq \frac{1}{8} \|f\|_{L^\infty} \implies \max_{P \in \mathbb{G}} |V_P| \leq \frac{1}{8} \|f\|_{L^\infty},$$

which confirms L^∞ -stability.

1.5 Consistency and convergence

Now that we have proven stability, we need to show consistency in order to find an error bound. A scheme is consistent if the local truncation error

$$\tau_P = \mathcal{L}_h u_P - \mathcal{L} u_P \rightarrow 0, \quad h \rightarrow 0.$$

From our derivation of the scheme we know that the truncation error is $O(h^2)$, and hence that consistency is satisfied. Since all third derivatives of the Taylor expansion cancel, we only need to look at the fourth derivatives to find an upper bound for the truncation error.

$$\begin{aligned} \tau_P &= \tau_{\vec{d}_1} + \tau_{\vec{d}_2} = \frac{ah^2}{12} \partial_x^4 u + \frac{2}{24} (h \partial_x + 2h \partial_y)^4 u \\ &= \frac{1+a}{12} h^2 \partial_x^4 u + \frac{2}{3} h^2 \partial_x^3 \partial_y u + 2h^2 \partial_x^2 \partial_y^2 u + \frac{8}{3} \partial_x \partial_y^3 u + \frac{4}{3} h^2 \partial_y^4 u + O(h^4). \end{aligned}$$

Using the stability result and the error equation, $e_P = U_P - u_P \Rightarrow -\mathcal{L}_h e_P = -\tau_P \Rightarrow |e_P| \leq \frac{1}{8} \|\tau_P\|_{L^\infty}$, we find that an error bound on the scheme in L^∞ is

$$|e_P| \leq \frac{1+a}{96} h^2 \max_{\Omega} |\partial_x^4 u| + \frac{1}{12} h^2 \max_{\Omega} |\partial_x^3 \partial_y u| + \frac{1}{4} h^2 \max_{\Omega} |\partial_x^2 \partial_y^2 u| + \frac{1}{3} h^2 \max_{\Omega} |\partial_x \partial_y^3 u| + \frac{1}{6} h^2 \max_{\Omega} |\partial_y^4 u|$$

Hence we see that for sufficiently smooth solutions, i.e. those that are 4 times differentiable with respect to x and y , the convergence is quadratic.

1.6 Convergence and testing

To test the convergence of our scheme, we use that any sufficiently smooth function $u(x, y)$ will be a solution given adapted right hand side $f(x, y)$ and boundary conditions. We only test for one example here, but the results of a different example is added in the appendix. Now, choosing $u(x, y) = \cos x \sin y$, we insert into (1) to find the RHS.

$$f(x, y) = 4 \cos y \sin x + (a+1) \cos x \sin y + 4 \cos x \sin y$$

Here, we have used $r = 2$. The boundary conditions quite simply become $u(x, y)$ (the analytic solution) at the different edges of our domain. Using this RHS and these boundary conditions in our solver, we plot the result and compare to the analytic solution $u(x, y)$. The results (displayed in Figure 4) look very promising. However, to get a more empirical view of the convergence we use different stepsizes and compare the result from our solver to the analytic solution using the max-norm. The results are shown in Figure 5.

The result of our convergence test for the numerical scheme applied to Fourier's law is consistent with our previous theoretical analysis. Our numerical test produced a convergence rate of 2.003, which was close to the theoretical value of 2 for a second-order accurate method. This indicates that our numerical method is able to approximate solutions to Fourier's law with high accuracy, and that the error decreases quadratically as the step size is reduced.

1.7 Irrational stepsize, $k = |r|h$

We now look at having $r \neq 2$ and irrational, also making $k = |r|h$ irrational. Since $y = nk$ with $n \in \mathbb{N}$ for all points on the grid, $y = 2$ is no longer a part of the grid. To overcome this problem we implement the method of fattening the boundary, which allows us to keep the same stencil for all $P \in \mathbb{G}$. This involves adapting the boundary contributions in the points closest to $y = 2$. For all points here, one step of length k in y -direction means we step outside Ω . Therefore we assume that the points just above $y = 2$ take the same value as the closest point on the boundary, where the solution is known. This is illustrated in figure 6.

We test convergence of the scheme in 3 different interesting cases: 1) With $r = \pi$ in which case the boundary $y = 2$ most likely is missed by quite a bit. Here we expect a slower convergence than $O(h^2)$, which is what we saw when we did not flatten the boundary. Since we increase M by a factor of 2 each step, we risk overshooting the boundary by the same amount even though the step size is reduced, which should show on the convergence plot as a sort of "jagged" behavior. 2) When r is chosen so that the last step barely surpasses $y = 2$. Here, we expect the error to be small and converge quadratically, as the approximation we perform at the boundary is small. 3) We overshoot $y = 2$ by almost an entire steplength. In this case we would expect the error to be at its largest, and converge the slowest.

As we see in figure 7, the results are coherent with what we expected. For case 2 and 3 the convergence is 1.992 and 0.977, i.e. quadratic and linear, respectively. For the "arbitrary" situation (case 1), we chose $r = \pi$, and here the convergence is spoiled. As explained, this is because reducing the step length by half not necessarily reduces the amount we overshoot the boundary, and hence the maximum error will not decrease when this is the case.

As expected, the error (as plotted in figure 8) increases substantially as we approach the boundary where we make an approximation. Compared to the result when we had $r = 2$, shown in figure 4, we clearly see that the new boundary approximation leads to an increased error, which is coherent with theory.

2 Isotropic Heat Distribution on an Irregular Domain

2.1 Problem definition and grid

We now define a new domain Ω to be the area enclosed by the parabola $y = 1 - x^2$ in the first quadrant. Our domain thus has the boundaries $\gamma_1 = [0, 1] \times 0$, $\gamma_2 = 0 \times [1, 0]$ and $\gamma_3 = \{(x, 1 - x^2) : x \in [0, 1]\}$

We now wish to solve the poisson equation in the isotropic case, i.e. where $\kappa = I$. Our equation then simplifies to

$$\Delta T = (\delta_x^2 + \delta_y^2)T = -f$$

2.2 Discretization and implementation

Since we here no longer need to worry about mixed derivatives we simply use central differences for both directional derivatives, and get the discretized equation

$$-\mathcal{L}_h u_P = \frac{1}{h^2} (-u_W + 4u_P - u_E - u_N - u_S)$$

This discretization results in a square grid with a 5-point stencil, but because of our irregular domain we can no longer ensure that for all center points U_P , every stencil point will be contained in our domain. We therefore need a way to deal with stencil points lying outside our domain. Here, we will implement and experiment with two different methods:

- 1) Modifying the discretization:

In cases where some stencil points lie outside our domain, we resolve this by locally changing our stencil. Instead of using the points outside our domain, we find the closest point along its "stencil arm" that is located on the boundary (shown in Figure 9). This implies finding some coefficient $\eta \in (0, 1)$, such that the new stencil point lying on the boundary is ηh length away from the center point. Given our domain, it will only be necessary to consider East and North points, as South and East points never will be outside Ω if $P \in \mathbb{G}$. In general, our scheme will then be

$$-\mathcal{L}_h u_P = \frac{-1}{h^2} (a_W u_W + a_P u_P + a_E u_E + a_N u_N + a_S u_S) \quad (6)$$

To achieve consistency, we need to do another Taylor expansion and determine the coefficients such that $\tau_P = O(h)$. Using similar notation as done in section 2.1, the Taylor expansions for the stencil points result in

$$\begin{aligned} a_W u_W &= a_W (u - h\partial_x u + \frac{1}{2}h^2\partial_x^2 u + O(h^3)). \\ a_S u_S &= a_S (u - h\partial_y u + \frac{1}{2}h^2\partial_y^2 u + O(h^3)). \\ a_{N'} u_{N'} &= a_{N'} (u + h\eta_1 \partial_y u + \frac{1}{2}(\eta_1 h)^2 \partial_y^2 u + O(h^3)). \\ a_{E'} u_{E'} &= a_{E'} (u + h\eta_2 \partial_x u + \frac{1}{2}(\eta_2 h)^2 \partial_x^2 u + O(h^3)). \end{aligned}$$

To have $\tau_P = O(h)$, we need that terms involving u , $\partial_x u$ and $\partial_y u$ sum to zero, and that terms involving $\partial_x^2 u$ and $\partial_y^2 u$ sum to one. This gives us the following set of equations and results:

$$\begin{cases} a_P + a_{N'} + a_{E'} + a_S + a_W = 0 \\ h(-a_W + \eta_2 a_{E'}) = 0 \\ h(-a_S + \eta_1 a_{N'}) = 0 \\ \frac{h^2}{2}(-a_S + \eta_1^2 a_{N'}) = 1 \\ \frac{h^2}{2}(a_W + \eta_2^2 a_{E'}) = 1 \end{cases} \implies \begin{cases} a_{N'} = \frac{2}{h^2} \frac{1}{\eta_1(1+\eta_1)} \\ a_{E'} = \frac{2}{h^2} \frac{1}{\eta_2(1+\eta_2)} \\ a_S = \frac{2}{h^2} \frac{1}{1+\eta_1} \\ a_W = \frac{2}{h^2} \frac{1}{1+\eta_2} \\ a_P = \frac{-2}{h^2} \frac{\eta_2 + \eta_1}{\eta_1 \cdot \eta_2} \end{cases}$$

Having found these coefficients, we can solve our system of equations for the inner nodes of our grid. Note here that if all stencil points $Q \in \Omega$, then $\eta_1 = \eta_2 = 1$ and we get our normal stencil.

2) Fattening the boundary:

Another method for handling general domains is by fattening the boundary. As explained in section 1.7, the main idea here is to expand our domain such that all stencil points will be within our enlarged domain, and use the same stencil for all inner points. We are then left with the question of what values should be assigned to the stencil points that may lie outside our domain. In our implementation, we have chosen to use the normal projection from the given point outside our domain, onto the boundary γ_3 (as shown in Figure 10). We can find this projection point analytically from any point $\vec{x} = (x_P, y_P)$ in the first quadrant. It can be shown that the projection point $\vec{x}_Q = (r, 1 - r^2)$, where r is a positive solution of $x_P + r(1 - y_P) - 2r^3 = 0$. Out of the two methods discussed, fattening the boundary is the easiest one to implement. This is because we do not need to alter our original scheme for boundary points.

2.3 Results from experimentation

Having implemented our two methods of handling irregular domains, we see that our methods seem to work in application. Similarly to what we did in section 1.6, we test for our scheme for a sufficiently smooth function $u(x, y)$, with an adapted RHS $f(x, y)$ and boundary conditions. Here we will only discuss the test example

$$u(x, y) = -\frac{1}{2\pi^2} \cos \pi x \cos \pi y = g(x, y), \quad f(x, y) = -\cos \pi x \cos \pi y$$

Having plotted the result and the exact solution in figure 11 with $M = 50$, we see that our numerical scheme seem to work quite well in both methods of handling the irregular boundary. From this plot it is clear that fattening the boundary makes its greatest error along the irregular boundary. This makes sense, as we have to estimate the value of the points outside the domain. For modifying the discretization the error is much smaller, and the largest error is not at the boundary.

We once again are interested in the convergence rate for both methods. Theoretically, we know that both methods should converge as $O(h)$ at the boundary. We create convergence plots, shown in Figure 12. For fattening the boundary we get a rate of 0.974, which is reasonably close to linear (which is what was expected). For modifying the boundary we get a result of 1.999, meaning approximately a quadratic convergence. This can be explained by the fact that the largest error was in the inner points, instead of being near the boundary. Since we check convergence by max-error, we will only measure convergence for interior points; not the boundary.

3 Conclusion

In summary, this project examined the effectiveness of finite differences methods in solving Fourier's law. The first part of the study involved the modeling and discretization of an anisotropic material, which resulted in the establishment of an error bound for the method. Through the use of a "test solution," the expected order of convergence of $O(h^2)$ was confirmed. Moreover, the study investigated the use of irrational step sizes and boundary modifications through "fattening," which yielded convergence results consistent with theoretical predictions.

The second part of the study assumed an isotropic material and solved Fourier's law on an irregular domain using both fattening and boundary modification techniques. Fattening yielded results close to the expected order of convergence of $O(h)$, while the modified boundary method had its largest error in the interior, and followed therefore a quadratic convergence.

Appendix

A Plots/figures

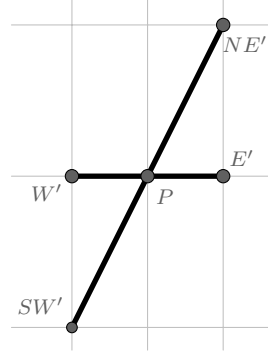


Figure 1: The stencil of our scheme.

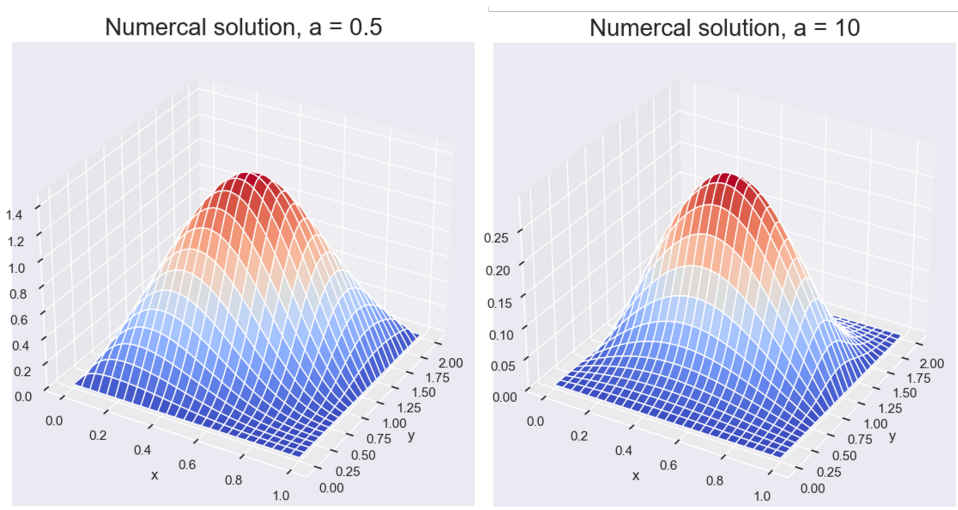


Figure 2: Comparison of numerical solution with same RHS but different values for a . $M = 52$.

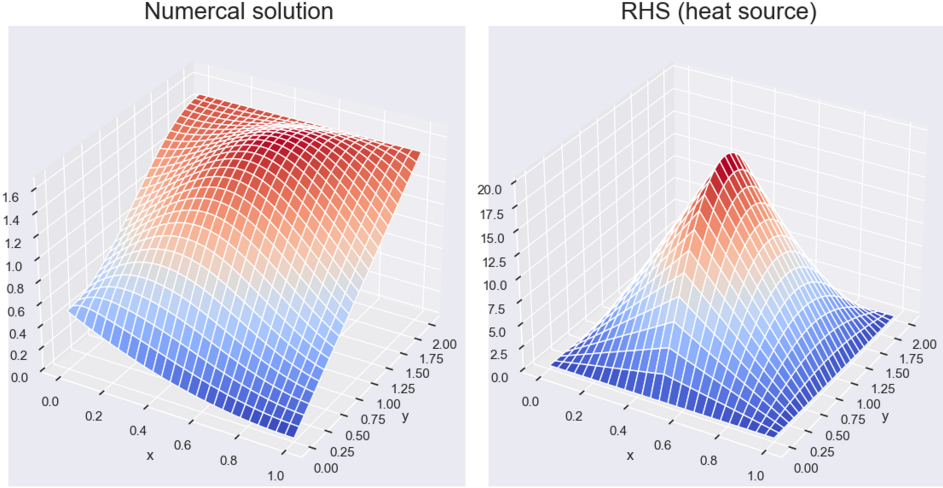


Figure 3: Numerical solution given RHS shown in right plot (hat function in x and trigonometric in y) and boundary conditions shown at boundaries in left plot. $M = 52$.

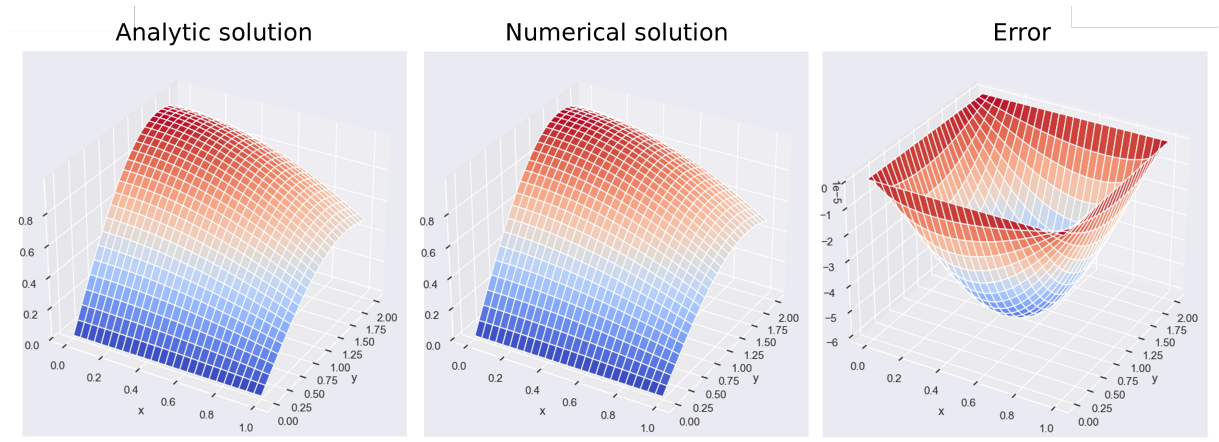


Figure 4: Comparison of analytic solution $u(x, y) = \cos x \sin y$ and our solver. The error-plot is produced by taking the difference. $M = 52$.



Figure 5: Convergence of numerical differences scheme for Fourier's law in anisotropic material. The error is calculated by the max norm of the difference to the analytic solution. The order is calculated by a linear curve-fit to the log-log plot.

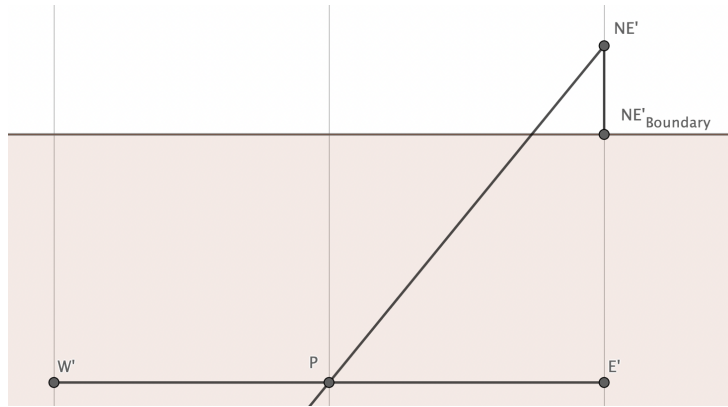


Figure 6: Fattening the boundary at $y = 2$.

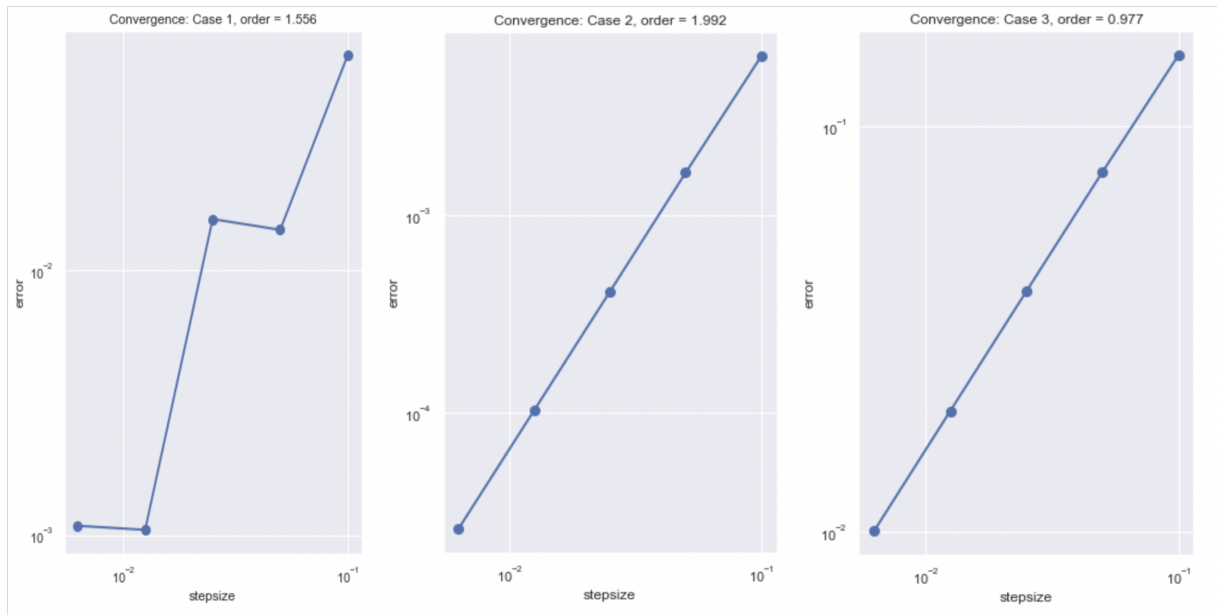


Figure 7: Convergence plot for rectangular domain, irrational r for the 3 cases described. Case 1: $r = \pi$. Case 2: $r = 4\frac{\pi+\delta}{\pi}$. Case 3: $r = 4\frac{\pi-\delta}{\pi}$. We set $\delta = 10^{-6}$.

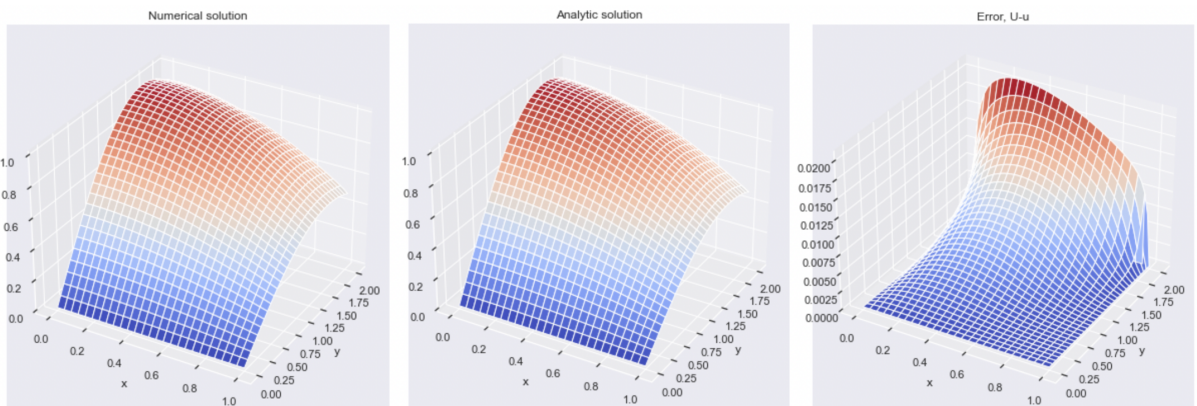


Figure 8: Analytic solution, numerical solution and error, $u(x, y) = \cos x \sin y$, $r = \pi$, $M = 50$.

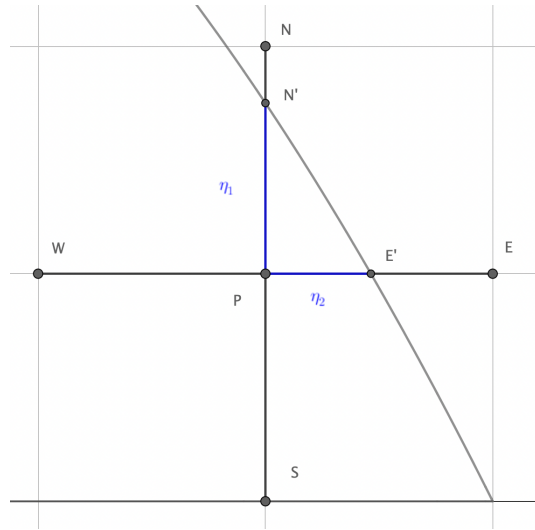


Figure 9: The stencil of our scheme when we fatten the boundary.

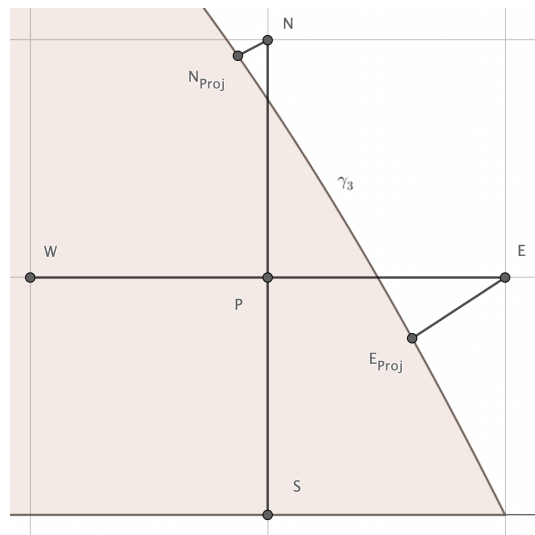


Figure 10: Stencil of our scheme when we modify the discretization at the boundary.

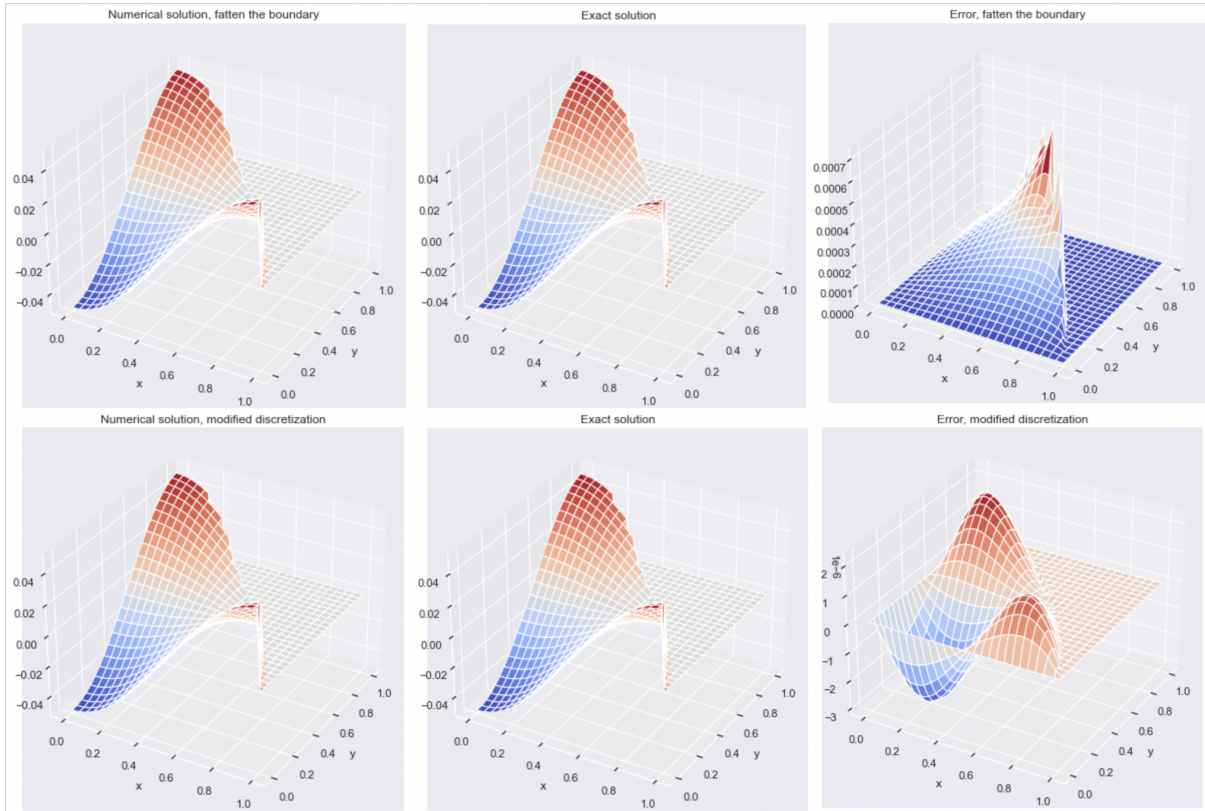


Figure 11: Solutions and error in the two methods discussed.

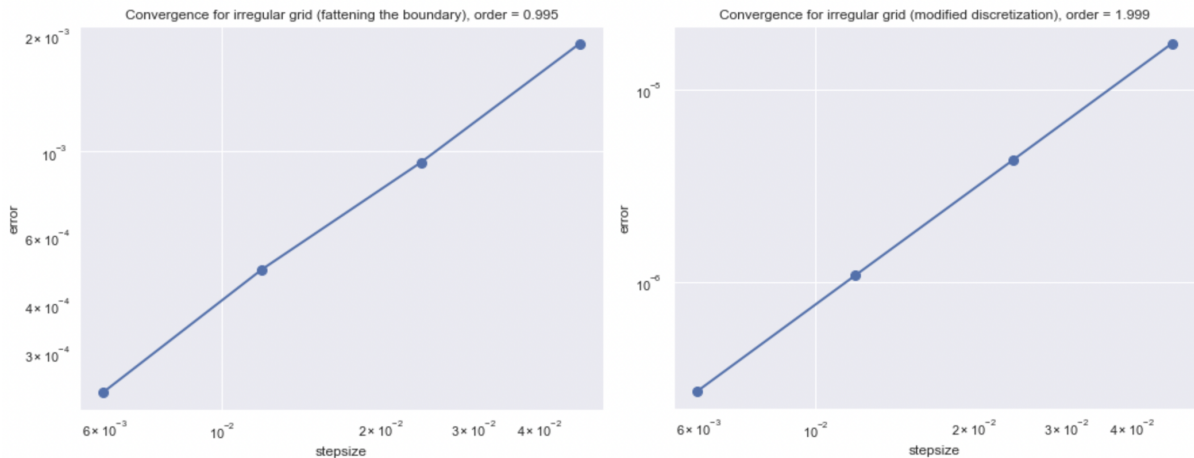


Figure 12: Convergence plot for the two methods of handling boundary errors